8-1 PARABOLOIDAL REFLECTOR GEOMETRY

Figure 8-1 shows the geometry of the parabolic reflector. We form the reflector by rotating the figure about its axis or by moving the figure along an axis out of the paper to form a cylindrical reflector. Because the cylindrical reflector requires a line source, it is less important than the circularly symmetrical reflector fed from a single point source. A paraboloidal reflector transforms a spherical wave radiated by the feed located at its focus into a plane wave. Although the feed wave spreads from the focus, which reduces its amplitude, geometric optics predicts a plane wave reflection that remains constant. The reflected wave does not remain a plane wave but spreads because the fields must be continuous across the reflection boundary of the beam plane wave column because fields can be discontinuous only across physical boundaries. Nevertheless, we will use the aperture theory on the projected diameter to predict its performance. Since the reflected rays are parallel, we can place the aperture plane anywhere along the axis, but somewhat close in front of the reflector. The equations for the reflector surface are

$$\underset{\substack{\text{rectangular}\\\text{coordinates}}}{r^2 = 4f(f+z)} \qquad \underset{\substack{\text{polar}\\\text{coordinates}}}{\rho = \frac{f}{\cos^2(\psi/2)}} \tag{8-1}$$

where f is the focal length, D the diameter, ρ the distance from the focus to the reflector, and ψ the feed angle from the negative z-axis. The reflector depth from the rim to the center is $z_0 = D^2/16f$.

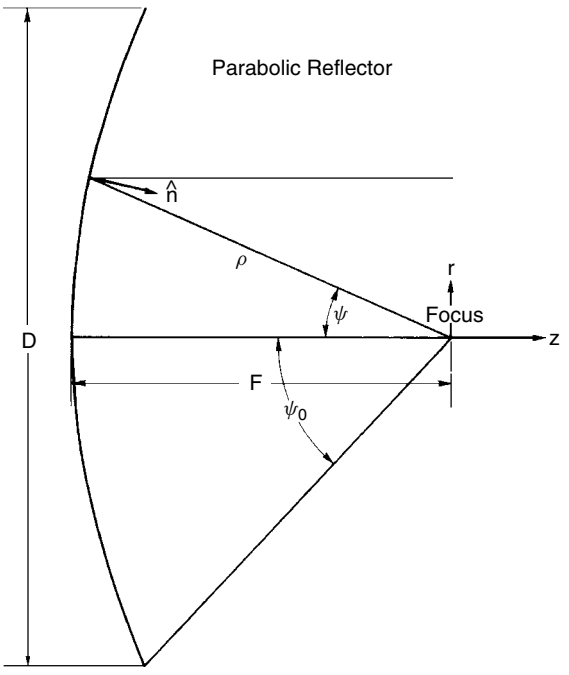

FIGURE 8-1 Geometry of a parabolic reflector.

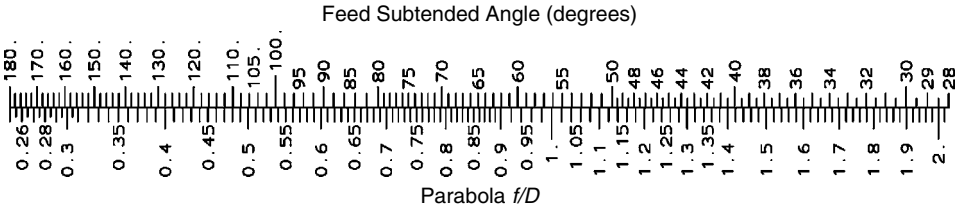

SCALE 8-1 Parabola f/D compared to a feed total subtended angle.

We eliminate the dimensions of the reflector by using the ratio f/D. The half subtended angle of the reflector, ψ_0, relates to f/D by

$$\psi_0 = 2\tan^{-1}\frac{1}{4f/D} \tag{8-2}$$

Scale 8-1 computes the total feed subtended angle from reflector f/D. When we place the aperture plane at the focus, the ray path distance becomes

$$\rho + \rho\cos\psi = 2\rho\cos^2\frac{\psi}{2} = 2f$$

all ray path lengths are equal, and the aperture plane is a constant-phase surface (eikonal).

The normal unit vector at a point on the reflector (r, z) is found from the feed angle:

$$\hat{\mathbf{n}} = -\sin\frac{\psi}{2}\hat{\mathbf{r}} + \cos\frac{\psi}{2}\hat{\mathbf{z}}$$

At this point we need the radius of curvatures in the principal planes to apply Eq. (2-77) reflection from a curved surface: R_1 in the $r-z$ plane and R_2 in the $\phi-z$ plane:

$$R_1 = \frac{2f}{\cos^3(\psi/2)} \quad \text{and} \quad R_2 = \frac{2f}{\cos(\psi/2)}$$

The spherical wave spreads from the feed as $1/\rho$. At the surface of the reflector the wave curvature changes to a plane wave and propagates to the aperture plane at a constant amplitude. The spherical wave spreading multiplies the feed distribution by [Eq. (8-1)] $\cos^2(\psi/2)$ in the aperture. Then

$$\text{added edge taper} = \cos^2\frac{\psi_0}{2} \qquad \text{voltage} \tag{8-3}$$

Deeper reflectors (smaller f/D) have greater edge tapers than shallow reflectors (larger f/D). Scale 8-2 provides a quick calculation of the added edge taper due to spherical wave spreading.

Example Calculate the edge taper of a paraboloidal reflector for $f/D = 0.5$ and an isotropic feed.

From Eq. (8-2), $\psi_0 = 2\tan^{-1}\frac{1}{2} = 53.13°$. The edge taper is [Eq. (8-3)]

$$\text{edge taper} = 20\log\cos^2\frac{53.13°}{2} = -1.94\,\text{dB}$$

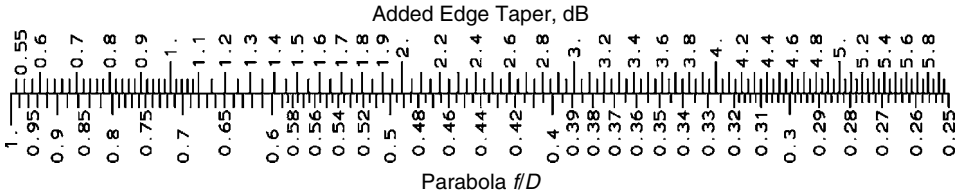

SCALE 8-2 Added edge taper due to a spherical wave from feed.

If the feed has its 10-dB pattern point directed toward the reflector edge, the aperture edge taper is 11.9 dB.

8-2 PARABOLOIDAL REFLECTOR APERTURE DISTRIBUTION LOSSES

We manipulate Eq. (4-2) for ATL to eliminate the dimensions and relate the integrals to the feed pattern:

$$\text{ATL} = \frac{\left[\int_0^{2\pi}\int_b^a \left|E_a(r',\phi')\right| r'\,dr'\,d\phi'\right]^2}{\pi a^2 \int_0^{2\pi}\int_b^a \left|E_a(r',\phi')\right|^2 r'\,dr'\,d\phi'} \tag{8-4}$$

where a is the aperture radius, b the central blockage radius, and $E_a(r', \phi')$ the aperture field. We make the following substitutions into Eq. (8-4):

$$\begin{aligned} r' &= \rho \sin\psi = 2\sin\frac{\psi}{2}\cos\frac{\psi}{2}\frac{f}{\cos^2(\psi/2)} = 2f\tan\frac{\psi}{2} \\ dr' &= f\sec^2\frac{\psi}{2} = \rho\, d\psi \end{aligned} \tag{8-5}$$

The aperture field is related to the feed pattern by

$$E_a(r',\phi') = \frac{E(\psi',\phi')}{\rho}$$

These substitutions eliminate dimensions in Eq. (8-4):

$$\text{ATL} = \frac{\left[\int_0^{2\pi}\int_{\psi_b}^{\psi_0} |E(\psi,\phi)|\tan(\psi/2)\,d\psi\,d\phi\right]^2}{\pi[\tan^2(\psi_0/2) - \tan^2(\psi_b/2)]\int_0^{2\pi}\int_{\psi_b}^{\psi_0} |E(\psi,\phi)|^2 \sin\psi\,d\psi\,d\phi} \tag{8-6}$$

where $\psi_b = 2\tan^{-1}[b/(2f)]$. When we substitute the relations in Eq. (8-5) into Eq. (4-9) to eliminate dimensions in the integrals, we obtain an expression with only the feed

pattern:

$$\text{PEL} = \frac{\left| \int_0^{2\pi} \int_{\psi_b}^{\psi_0} E(\psi, \phi) \tan(\psi/2)\, d\psi\, d\phi \right|^2}{\left[\int_0^{2\pi} \int_{\psi_b}^{\psi_0} |E(\psi, \phi)| \tan(\psi/2)\, d\psi\, d\phi \right]^2} \tag{8-7}$$

PEL is the efficiency at the boresight. We modify Eq. (8-7) when we scan the beam to give off-boresight values as in Eq. (4-3).

The amplitude taper efficiency (ATL) of Eq. (8-6) and the phase error efficiency (PEL) of Eq. (8-7) do not account for the total directivity loss of the aperture. The reflector does not intercept all the power radiated by the source and some of it spills over the edge. Spillover adds little to the pattern except as sidelobes, since usual feeds have small backlobes. We consider this spilled-over power as a loss (SPL):

$$\text{SPL} = \frac{\int_0^{2\pi} \int_{\psi_b}^{\psi_0} |E(\psi, \phi)|^2 \sin\psi\, d\psi\, d\phi}{\int_0^{2\pi} \int_0^{\pi} |E(\psi, \phi)|^2 \sin\psi\, d\psi\, d\phi} \tag{8-8}$$

This expression for spillover includes the scattered portion of the central blockage efficiency, but not the loss of potential aperture. We include the remainder in the directivity calculation.

We have ignored the cross-polarized power radiated by the source. We define cross-polarization efficiency (XOL) as

$$\text{XOL} = \frac{\int_0^{2\pi} \int_0^{\pi} |E_C(\psi, \phi)|^2 \sin\psi\, d\psi\, d\phi}{\int_0^{2\pi} \int_0^{\pi} (|E_C(\psi, \phi)|^2 + |E_X(\psi, \phi)|^2) \sin\psi\, d\psi\, d\phi} \tag{8-9}$$

where E_c is the co-polarized field and E_x is the cross-polarized field. These polarizations correspond to Ludwig's [10] third definition of cross-polarization. A Huygens source produces straight reflector surface currents when projected to the aperture plane. Including the cross-polarization efficiency gives us the true average radiation intensity as in Eq. (1-17).

If we express the efficiencies as ratios, the directivity will be found from

$$\text{directivity} = \left(\frac{\pi}{\lambda}\right)^2 (D_r^2 - D_b^2)\text{SPL} \cdot \text{ATL} \cdot \text{PEL} \cdot \text{XOL} \quad \text{(ratio)} \tag{8-10}$$

where D_r is the reflector diameter and D_b is the diameter of the central blockage. Equation (8-10) includes the nonscattered blockage loss of potential aperture. Equation (8-10) can be expressed in terms of decibel ratios:

$$\begin{aligned} \text{directivity} = 10\log\left[\left(\frac{\pi}{\lambda}\right)^2 (D_r^2 - D_b^2)\right] + \text{SPL(dB)} + \text{ATL(dB)} \\ + \text{PEL(dB)} + \text{XOL(dB)} \end{aligned} \tag{8-11}$$

Of course, all the decibel ratios of the efficiencies will be negative and subtract from the directivity calculated from the area.

When measuring an actual feed, we can ignore the cross-polarized power. We measure the efficiency as the difference between directivity and gain. Actual directivity includes the co-polarizations and cross-polarizations in the average radiation intensity. If we ignore the cross-polarization, the measured efficiency decreases by the cross-polarization loss because the measured and true directivity differ by that loss. We must measure the cross-polarization pattern distribution of the feed if we want to calculate the cross-polarized secondary (reflector) pattern. When the cross-polarization pattern is not required, we save time without loss of accuracy by measuring only the co-polarized feed pattern.

Equations (8-8) and (8-9) are by no means unique. We could include the cross-polarized power in the spillover calculation [Eq. (8-8)] and limit the integration limits in Eq. (8-9) to the reflector. A set of efficiency relations is correct when the equations account for all the power radiated by the feed. When we use calculated feed patterns, we must determine cross-polarization efficiency, since we can only estimate the efficiency due to material losses. The cross-polarization efficiency cannot be included as it is in measurements, and the division of cross-polarized power between Eqs. (8-8) and (8-9) is arbitrary.

8-3 APPROXIMATE SPILLOVER AND AMPLITUDE TAPER TRADE-OFFS

We use the approximate pattern $\cos^{2N}(\psi/2)$ for a feed pattern to establish trends. Of course, if the actual feed pattern distribution is available, we should use Eqs. (8-6) to (8-9). We obtain closed-form expressions when we substitute this pattern into Eqs. (8-6) and (8-8). Ignoring any central blockage, we get

$$\text{spillover efficiency} = 1 - u^{2(N+1)} \tag{8-12}$$

$$\text{amplitude taper efficiency} = \frac{4(N+1)(1-u^N)^2}{N^2[1-u^{2(N+1)}]} \cot^2 \frac{\psi_0}{2} \tag{8-13}$$

where $u = \cos(\psi_0/2)$. We combine Eqs. (8-12) and (8-13) and plot their combination to find the beamwidth for minimum loss. In Figure 8-2 the loss versus the 10-dB beamwidth for various f/D values is plotted. At narrow beamwidths little feed power spills over the reflector edge, but the reflector is underilluminated. Increasing the beamwidth improves the illumination but increases the spillover. The efficiency peaks when the feed 10-dB beamwidth is approximately the subtended angle of the reflector. Figure 8-2 shows a broad peak for any given f/D. Small changes in the beamwidth near the peak have no practical effect on the reflector's gain. Scale 8-3 relates the average illumination loss reduction given the feed pattern level in the direction of the reflector rim for typical antennas.

Example Estimate the amplitude taper loss for a reflector with $f/D = 0.5$ whose feed has a 10-dB edge taper.

Compare the loss with that of the circular Gaussian and the Hansen single-parameter distributions: $\psi_0 = 2\tan^{-1}\frac{1}{2} = 53.13^\circ$. The 10-dB beamwidth of the feed is then 106.26°. We modify Eq. (1-20) to compute the exponent N of the $\cos^{2N}(\psi/2)$ feed

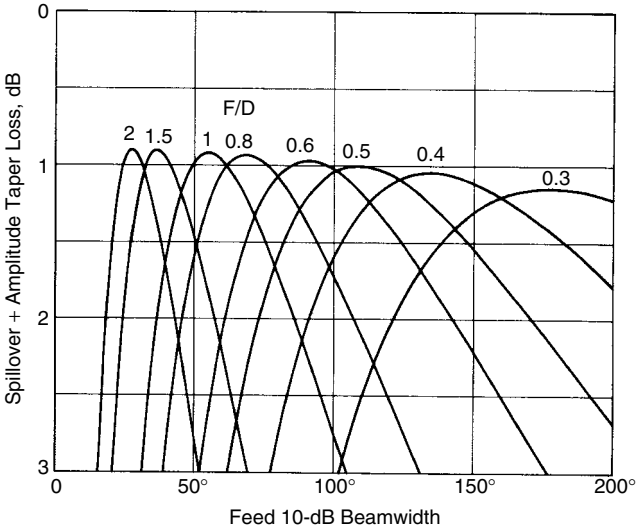

FIGURE 8-2 Sum of spillover and amplitude taper losses versus feed 10-dB beamwidth.

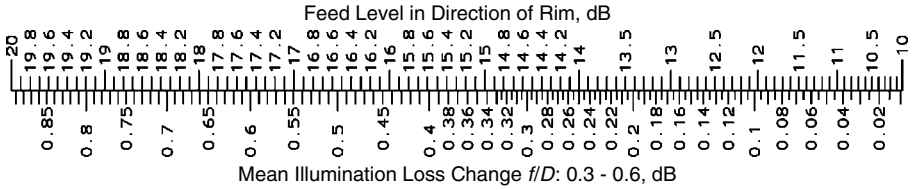

SCALE 8-3 Mean illumination loss change of a reflector given the feed pattern level in the rim direction.

pattern approximation,

$$N = \frac{\log 0.1}{2 \log \cos(106.26^\circ/4)} = 10.32$$

From Eq. (8-13), $u = \cos(53.13^\circ/2) = 0.894$:

$$\text{ATL(dB)} = \frac{4(1 - 0.894^{10.32})^2(11.32)}{10.32^2(1 - 0.894^{22.64})} \cot^2(53.13^\circ/2) = 0.864$$
$$= 10 \log 0.864 = -0.63 \text{ dB}$$

The extra distance from the feed to the reflector edge compared with the center distance adds 1.94 dB and increases the aperture amplitude taper to 11.94 dB. We interpolate Table 4-29 for the circular Gaussian distribution and Table 4-30 for the Hansen single-parameter distribution to find the following data:

Gaussian	Hansen
ATL(dB) = −0.62 dB	ATL(dB) = −0.57 dB
Sidelobe level = 26.3 dB	Sidelobe level = 24.7 dB
Beamwidth factor = 1.142	Beamwidth factor = 1.136

We multiply Eq. (4-83) by the beamwidth factor to estimate the reflector beamwidth:

$$\text{HPBW} = 67.3^\circ \frac{\lambda}{D} \quad \text{and} \quad \text{HPBW} = 67^\circ \frac{\lambda}{D}$$

These compare well with the approximation, $\text{HPBW} = 70^\circ\lambda/D$ for a parabolic reflector. An integration of the aperture distribution for the far-field pattern gives the following results:

$$\text{HPBW} = 67.46^\circ \frac{\lambda}{D} \qquad \text{sidelobe level} = 27\,\text{dB}$$

8-4 PHASE ERROR LOSSES AND AXIAL DEFOCUSING

All rays starting at the reflector focus travel the same distance through reflection to the aperture plane. The aperture plane is any convenient plane in front of the dish whose normal is the axis of the reflector. If we could build a feed with a unique phase center and place it at the focus of a perfect paraboloidal reflector, we would eliminate phase error loss in the aperture plane because it would have a constant phase. The feed, the positioning of the feed, and the reflector surface all contribute to the phase error loss.

We discussed techniques for obtaining unique phase centers in the various planes for horns. Unlike smooth-wall horns, corrugated horns can have equal phase centers in all planes through the axis, but even their position will wander with changes in frequency. We measure the feed pattern distribution (amplitude and phase) to predict the contribution of the feed to the overall efficiency. From those measurements we define the practical phase center as the point on the feed leading to the minimum phase error loss when placed at the focus. The random and systematic phase error contributions can be measured directly on the feed and calculated numerically using Eq. (8-7).

The feed phase center cannot always be placed at the focus. The phase-center location wanders with changes in frequency, and in any wideband application we expect axial defocusing. For example, the location of the phase center of a log-periodic antenna moves toward the apex as frequency increases. Figure 8-3 is a plot of the phase error loss due to axial defocusing. Each feed has its 10-dB beamwidth equal to the reflector subtended angle. Axial defocusing affects deep dishes (lower f/D) more than shallow dishes. We can estimate the axial defocusing phase error loss by approximating the distribution with a quadratic aperture phase distribution. Given z as the axial defocusing, the maximum phase deviation in cycles is

$$S = \frac{z}{\lambda}\left[1 - \cos\left(2\tan^{-1}\frac{1}{4f/D}\right)\right] \tag{8-14}$$

We combine this with the quadratic phase error loss of the circular Gaussian distribution to estimate the loss. With $z = \lambda$ we obtain a scaling factor for S (Scale 8-4) given z from Eq. (8-14). The scaling factor decreases with increasing f/D.

Example Estimate the phase error loss for $z = 2\lambda$ when $f/D = 0.6$ and the feed 10-dB beamwidth equals the reflector subtended angle.

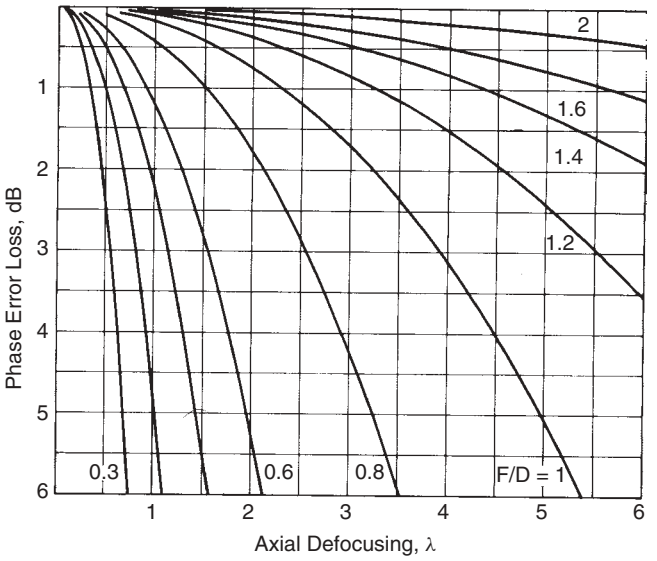

FIGURE 8-3 Paraboloidal reflector phase error loss due to axial defocusing of the feed.

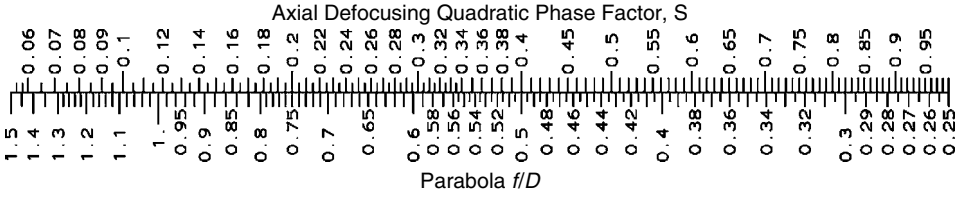

SCALE 8-4 Quadratic phase factor S for axial defocusing of a paraboloidal reflector.

From Scale 8-4, $S = 0.30(2) = 0.60$. We use Eq. (8-3) to compute the edge taper:

$$\psi_0 = 2\tan^{-1}\frac{1}{2.4} = 45.2^\circ$$

$$\text{edge taper} = 20\log\cos^2\frac{\psi_0}{2} = -1.4\,\text{dB}$$

An equivalent truncated Gaussian aperture distribution tapers to

$$10\,\text{dB} + 1.4\,\text{dB} = 11.4\,\text{dB} \qquad \rho = \frac{11.4}{8.69} = 1.31$$

We use Eq. (4-118) to calculate phase error efficiency of the truncated Gaussian distribution: PEL = 0.305 or PEL (dB) = −5.2 dB. This matches the value from Figure 8-3 found by integration of the actual distribution. The optimum feed beamwidth produces an average aperture edge taper of 11.8 dB. Scale 8-5 evaluates Eq. (4-118) for this taper.

We detect axial defocusing by looking at the patterns of the reflector. Axial defocusing fills-in nulls between sidelobes. We adjust the feed location to maximize the null

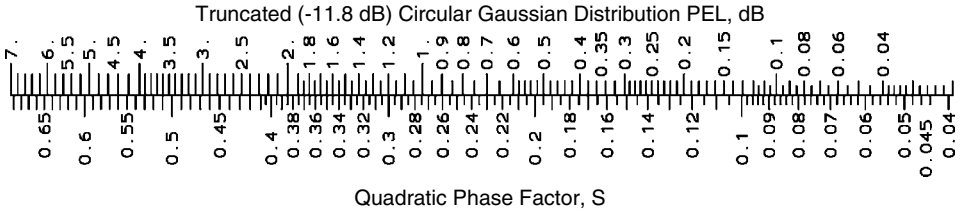

SCALE 8-5 Truncated circular Gaussian distribution (−11.8 dB taper) phase error loss given S.

depth, but antenna range errors and receiver sensitivity limit our ability to eliminate this defocusing.

8-5 ASTIGMATISM [11]

Both the feed and the reflector can have astigmatism: unequal phase centers in different planes. We measure the feed by itself to discover its astigmatism. When the feed is mounted in the reflector, we detect astigmatism by the depth of nulls in the various pattern planes. A series of measurements can separate the feed and reflector astigmatism, but the feed must be able to move along the reflector axis and to rotate by 90° during the measurements. Move the feed along the axis to find the locations that give maximum nulls. The extrema of the reflector focuses may not occur in the E- and H-planes and will require a search in the other planes. At this point we cannot separate the feed astigmatism from the reflector astigmatism. We rotate the feed and repeat the measurements. The feed phase center locations shift, and the reflector focuses remain fixed. Simple manipulation of the data from the two measurements separates the two sources of astigmatism. The reflector can be shimmed to remove its astigmatism, or the feed phase centers can be matched to the reflector focuses. Figure 8-4 shows the magnitude

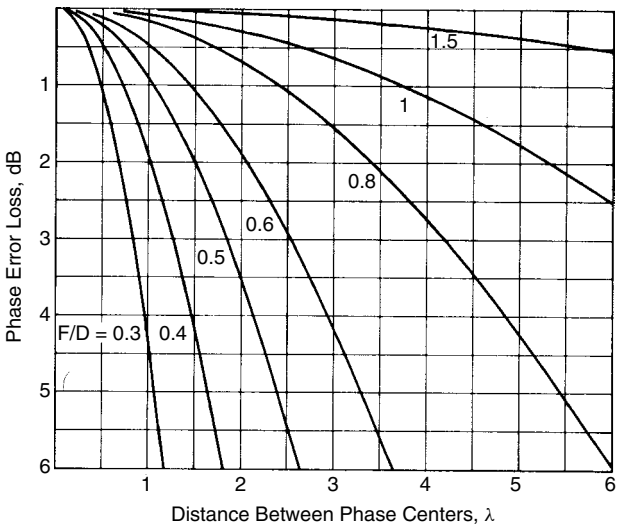

FIGURE 8-4 Paraboloidal reflector phase error loss due to feed astigmatism.

of phase error losses due to feed astigmatism. Astigmatism loss is not as severe as axial defocusing because in two planes the feed phase center is at the reflector focus. As is true of axial defocusing loss, deep dishes are affected more than shallow reflectors.

8-6 FEED SCANNING

Moving the phase center of the feed off axis laterally scans the reflector beam to a limited extent without severe pattern problems. Figure 8-5 shows the k-space pattern effects of feed scanning. The sidelobes show the effects of coma (cubic phase errors) where the sidelobes on the boresight side grow and the sidelobes on the other side decrease. We call these *coma lobes*, although no new lobes are generated. In fact, we see one lobe disappearing as a vestigial lobe with increased scan (Figure 8-5). Suppose that the feed is offset from the axis by a distance d. We measure the offset angle ψ_S from the axis to a line from the feed to the reflector vertex: $d = f \tan \psi_S$. We ignore the slight amplitude distribution change due to the small lateral offset. Referred to the focus, the movement produces a phase factor in the feed pattern: $-kd \sin \psi \cos \phi_c$ when the feed is moved along the negative x-axis.

Equation (8-7) predicts only the boresight phase error loss. Like Eq. (4-3), we must calculate the phase error efficiency at any angle to determine the loss at the pattern peak:

$$\mathrm{PEL}(\theta, \phi) = \frac{\left| \int_0^{2\pi} \int_0^{\psi_0} E(\psi, \phi_c) \tan(\psi/2) e^{jk2f \tan(\psi/2) \sin\theta \cos(\phi - \phi_c)} \, d\psi \, d\phi_c \right|^2}{\left[\int \int |E(\psi, \phi_c)| \tan(\psi/2) \, d\psi \, d\phi_c \right]^2} \tag{8-15}$$

When we include the offset along $\phi = 0$, the phase factor becomes

$$\exp\left[jkf \cos\phi_c \left(2 \tan \frac{\psi}{2} \sin\theta - \tan\psi_S \sin\psi \right) \right]$$

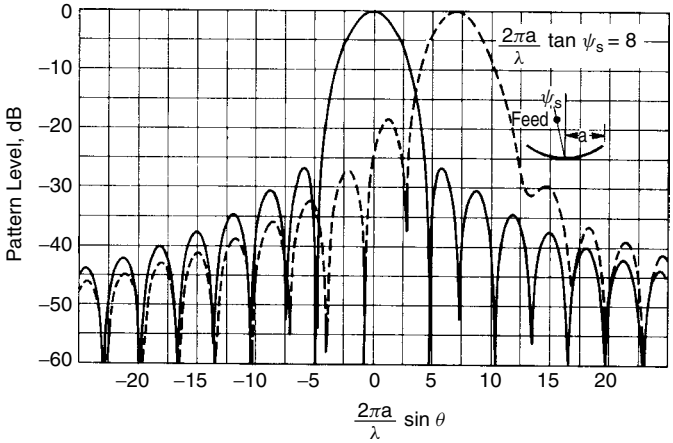

FIGURE 8-5 Feed-scanned paraboloidal reflector $f/D = 0.5$ and feed beamwidth $= 60^\circ$.

For large reflectors we make the approximations $\psi_S \approx \tan\psi_S$ and $\theta \approx \sin\theta$. The pattern scale and the offset phase factor become $ka\theta$ and $ka\psi_S$.

A flat plate would reflect the ray at an equal angle on the other side of the axis for an offset feed, but a curved reflector modifies that result slightly. The offset factor in Figure 8-5 is 8, and the beam peak is at 7. We call the ratio of the beam maximum to offset angle the beam deviation factor (BDF) [12]:

$$\text{BDF} = \frac{\theta_m}{\psi_S} = \frac{7}{8} \qquad \theta_m = \text{BDF} \cdot \psi_S$$

The BDF varies from less than 1 for a concave reflector to greater than 1 for a convex reflector. BDF equals 1 for a flat reflector. Table 8-1 lists the BDF values for various f/D and Scale 8-6 gives the relationship. The BDF approaches 1 as f/D approaches infinity (flat plate). The approximate expression for BDF is

$$\text{BDF} = \frac{(4f/D)^2 + 0.36}{(4f/D)^2 + 1} \tag{8-16}$$

Feed scanning increases the phase error loss. When normalized to beamwidths of scan, a single loss curve can be drawn for each f/D (Figure 8-6). Scanning also raises the sidelobes. Table 8-2 gives the approximate level of the peak coma lobe for a given scan loss. It is almost independent of f/D.

TABLE 8-1 Feed-Scanned Paraboloidal Reflector Beam Deviation Factor

f/D	BDF	f/D	BDF
0.30	0.724	0.80	0.945
0.35	0.778	0.85	0.951
0.40	0.818	0.90	0.957
0.45	0.850	1.00	0.965
0.50	0.874	1.10	0.970
0.55	0.893	1.20	0.975
0.60	0.908	1.40	0.981
0.65	0.921	1.60	0.986
0.70	0.930	1.80	0.989
0.75	0.938	2.00	0.991

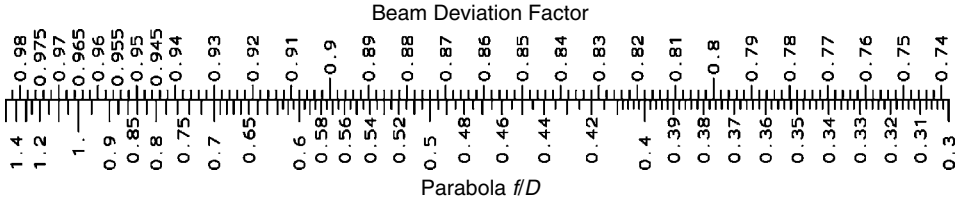

SCALE 8-6 Feed-scanned reflector beam deviation factor given f/D.

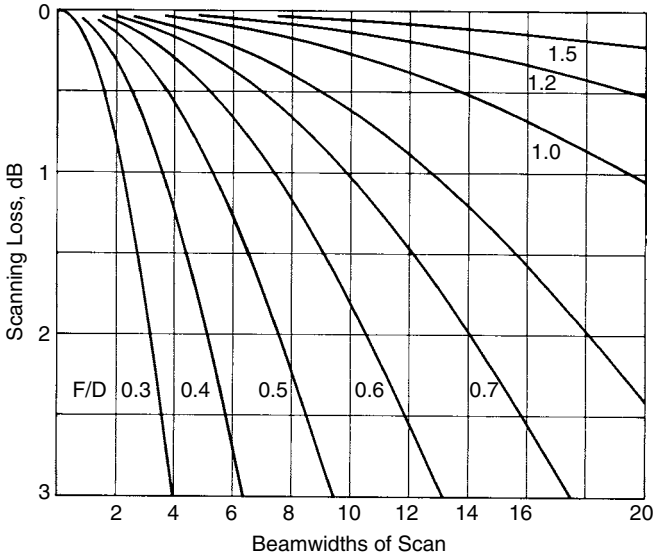

FIGURE 8-6 Feed-scanning loss of a paraboloidal reflector.

TABLE 8-2 Sidelobe Level of a Feed-Scanned Paraboloidal Reflector

Scanning Loss (dB)	Sidelobe Level (dB)	Scanning Loss (dB)	Sidelobe Level (dB)
0.50	14.1	1.75	10.1
0.75	12.9	2.0	9.7
1.00	11.9	2.5	9.0
1.25	11.2	3.0	8.5
1.50	10.6		

Example A reflector with a 50λ diameter is feed-scanned to 6°. Compute the offset distance and scanning loss when $f/D = 0.6$.

Use the approximation HPBW $= 70^\circ\lambda/D = 1.4^\circ$. The reflector is scanned $6/1.4 = 4.3$ beamwidths:

$$\text{scanning loss (Figure 8-6)} = 0.4\,\text{dB}$$

$$\text{sidelobe level (Table 8-2)} = 14.6\,\text{dB}$$

The angle between the axis and the feed point to vertex must be greater than the scan angle, since the reflector is concave:

$$\psi_S = \frac{\theta_S}{\text{BDF}} = \frac{6^\circ}{0.908} = 6.61^\circ \quad \text{(Table 8-1)}$$

The offset distance is $f \tan 6.61^\circ = 0.6(50\lambda) \tan 6.61^\circ = 3.48\lambda$.

The scalar analysis of this section gives only approximate results. Large feed scanning produces higher-order aberrations other than coma [13–15]. The optimum gain point moves off the focal plane but fails to follow the curve predicted from optics for reflectors extremely large in wavelengths [14]. The reflector f/D and illumination taper determine the maximum gain contour for feed-scanning a reflector. Vector analysis improves the match between calculated and measured results [15].

8-7 RANDOM PHASE ERRORS

Reflector anomalies reduce the gain predicted from the feed analysis. We must specify reasonable manufacturing tolerances for the frequency of operation. It would appear that gain can be increased without bound by increasing the reflector diameter, but the tolerance problems of large reflectors limit the maximum gain. We consider only surface anomalies so small that on average the reflector retains its basic shape. The surface imperfections change the optical path length from the feed to the reflector aperture plane by $\delta(r, \phi)$, which gives us

$$\text{PEL} = \frac{\left| \int_0^{2\pi} \int_0^a E(r, \phi) e^{j\delta(r,\phi)} r \, dr \, d\phi \right|^2}{\left[\int_0^{2\pi} \int_0^a |E(r, \phi)| r \, dr \, d\phi \right]^2} \tag{8-17}$$

Cheng [16] bounds the phase error loss by using a limit on the integrals. Given a peak phase error of m (radians), the change in gain is bounded:

$$\frac{G}{G_0} \geq \left(1 - \frac{m^2}{2}\right)^2 \tag{8-18}$$

This gain loss estimate is too conservative, but it is useful as an upper bound.

Ruze [17] improved the random surface error loss estimate by using a Gaussian distributed error correlated over regions. Dents or segments making up the reflector are correlated with the errors over a nearby region. The error at a point depends on the location of nearby points in the correlation region. The phase error efficiency becomes an infinite series:

$$\text{PEL} = \exp(-\overline{\delta}^2) + \frac{1}{\eta} \left(\frac{2C}{D}\right)^2 \exp(-\overline{\delta}^2) \sum_{n=1}^{\infty} \frac{(\overline{\delta}^2)^n}{n \cdot n!} \tag{8-19}$$

where C is the correlation distance, D the diameter, and η the aperture efficiency (ATL). $\overline{\delta}^2$ is the mean-square phase deviation, given by

$$\overline{\delta}^2 = \frac{\int_0^{2\pi} \int_0^a |E(r, \phi)| \delta^2(r, \phi) r \, dr \, d\phi}{\int_0^{2\pi} \int_0^a |E(r, \phi)| r \, dr \, d\phi} \tag{8-20}$$

If we include the correlation distance, PEL decreases. The infinite series [Eq. (8-19)] converges rapidly. When the correlation distance is small compared with the diameter, the phase error efficiency becomes

$$\text{PEL} = \exp\left(\frac{-4\pi\varepsilon_0}{\lambda}\right)^2 = \exp(-\bar{\delta}^2) \tag{8-21}$$

where ε_0 is the effective reflector tolerance. We use 4π instead of 2π because the wave travels to and from the reflector and the phase distance is twice the reflector tolerance. From Eq. (8-20) we derive the effective RMS tolerance:

$$\varepsilon_o^2 = \frac{\displaystyle\int_0^{2\pi}\int_0^a |E(r,\phi)|\varepsilon^2(r,\phi)r\,dr\,d\phi}{\displaystyle\int_0^{2\pi}\int_0^a |E(r,\phi)|r\,dr\,d\phi} \tag{8-22}$$

Ruze gives the distance ε in terms of the z-axis deviation Δz and the surface normal

$$\varepsilon = \frac{\Delta z}{1+(r/2f)^2} \qquad \varepsilon = \frac{\Delta n}{\sqrt{1+(r/2f)^2}} \tag{8-23}$$

We evaluate the constants in Eq. (8-21) and convert to a decibel ratio:

$$\text{PEL(dB)} = -685.8\left(\frac{\varepsilon_0}{\lambda}\right)^2 \tag{8-24}$$

Example Compute the required reflector tolerance at 30 GHz to limit the RMS surface tolerance phase error loss to 1 dB.

Using Eq. (8-24), we get

$$\frac{\varepsilon_0}{\lambda} = \sqrt{\frac{1}{685.8}} = 0.038$$

At 30 GHz, $\lambda = 1$ cm and $\varepsilon_0 = 0.38$ mm. We can also use Eq. (8-18), which gives the upper bound on surface error loss:

$$m = \frac{4\pi\varepsilon_0}{\lambda} = \sqrt{2\left(1-\sqrt{\frac{G}{G_0}}\right)} = 0.466 \text{ at } 1\text{ dB}$$

$\varepsilon_0 = 0.037\lambda$ or $\varepsilon_0 = 0.37$ mm at 30 GHz. Both methods give about the same answer in this case.

Zarghamee [18] extended tolerance theory to include the effects of the surface error distribution. Some antennas have better support and construction in some areas and are more accurate in those areas. This improves the reflector performance. Zarghamee defined a second variation of surface deviations by

$$\eta_0^4 = \frac{\displaystyle\int_0^{2\pi}\int_0^a |E(r,\phi)|[\varepsilon^2(r,\phi)-\varepsilon_0^2]r\,dr\,d\phi}{\displaystyle\int_0^{2\pi}\int_0^a |E(r,\phi)|r\,dr\,d\phi}$$

The phase error efficiency becomes

$$\text{PEL} = \exp\left(\frac{-4\pi\varepsilon_0}{\lambda}\right)^2 \exp\left(\frac{\pi\eta_0}{\lambda}\right)^4$$

The correlation of random errors increases the probable sidelobe level. The sidelobe level increases with the size of the correlation interval and decreases for larger aperture diameters. Increasing the amplitude taper of the distribution makes the aperture pattern more susceptible to random-error sidelobes, since increasing the taper is somewhat equivalent to decreasing the aperture diameter. Blockage and feed diffraction also limit the achievable sidelobe level in a reflector. A simple feed cannot carefully control the aperture distribution necessary for low sidelobes. Hansen [19, p. 74] discusses sidelobe limitations caused by random phase error in some detail.

Paraboloidal reflectors can be made in an umbrella shape where the ribs are parabolic and wire mesh is stretched between them [20]. The gore shape causes phase error loss and their periodicity produces extra sidelobes. Given the number of gores N_G and the focal length of the ribs f_r, the surface is given by

$$f(\psi) = f_r \frac{\cos^2(\pi/N_G)}{\cos^2\psi}$$

where ψ is measured from the centerline between the ribs. We calculate the average focal length by integrating across the gore half-angle π/N_G and dividing by π/N_G:

$$f_{\text{av}} = f_r \frac{\sin(2\pi/N_G)}{2\pi/N_G} \tag{8-25}$$

We use Eq. (8-25) to calculate the rib focal length given the average focal length of the reflector.

The peak sidelobe due to the periodic gores occurs at an angle θ_p found from the number of gores and the diameter D:

$$\theta_p = \sin^{-1}\left(1.2N_G\frac{\lambda}{\pi D}\right) \tag{8-26}$$

Given the average f/D of the reflector, we determine the peak-to-peak phase deviation across the gore by the approximate equation

$$\Delta = \frac{800 - 500(f/D - 0.4)}{N_G^2}\frac{D}{\lambda} \tag{8-27}$$

Scale 8-7 lists the phase error loss for a feed edge taper of 10 dB. Increasing the feed taper decreases the phase error loss due to gore construction. When we use a 20-dB feed taper, the values given by Scale 8-7 reduce by 0.16 dB for 0.5 dB of loss, 0.31 dB for 1 dB, and 0.45 dB for 1.5 dB. The gain losses due to underillumination by the 20-dB edge taper feed exceed these values.

Example Given a reflector with $D/\lambda = 35$ with a limit of 0.5 dB loss due to gore construction for $f/D = 0.34$, we discover that the allowable peak-to-peak phase error from Scale 8-7 is 124°. Using Eq. (8-27), we solve for the number of ribs:

$$N_G^2 = \frac{830}{124}35 = 234 \quad \text{or} \quad N_G = 16$$

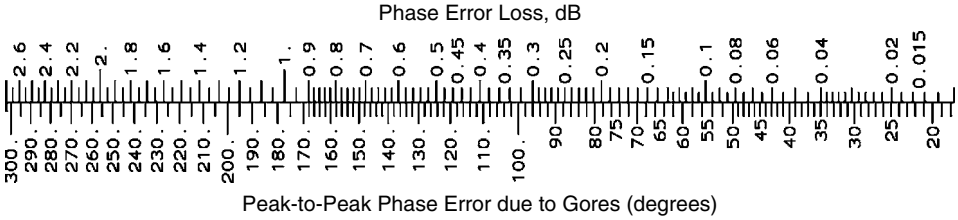

SCALE 8-7 Phase error loss due to gore construction of a paraboloidal reflector.

We use Eq. (8-26) to compute the angle of the peak gore sidelobe, $\theta_p = 10.0^\circ$. Equation (8-27) shows that the phase deviation Δ is proportional to frequency. If the frequency increases by 1.5 times, then by Eq. (8-27), 124° increases to 186° and we read 1.1 dB of loss from Scale 8-7 while the peak gore sidelobe becomes $\theta_p = 6.7^\circ$.

8-8 FOCAL PLANE FIELDS

We improve the efficiency and pattern response of a reflector if we match the feed fields to the focal plane fields. GO assumes a point focus, but an actual focus is extended. We determine the reflector and feed efficiency from the field match over the focal plane. When the reflector f/D value is large, we use the diffraction pattern of a circular aperture, the Airy function:

$$E = \frac{J_1(kr\psi_0)}{kr\psi_0} \tag{8-28}$$

where ψ_0 is the half subtended angle of the reflector (radians), r the radial coordinate, k the propagation constant, and J_1 the Bessel function.

In a more exact method the currents induced on the reflector ($2\mathbf{n} \times \mathbf{H}$) and the magnetic vector potential are used to calculate the focal plane fields. As f/D decreases, the currents on the reflector interact and modify their distribution, but it is a secondary effect [21]. Iterative physical optics analysis (section 2-4) can find these current modifications. We calculate the reflector efficiency from the field match of the focal plane fields ($\mathbf{E}_1$, $\mathbf{H}_1$) and the fields of the feed ($\mathbf{E}_2$, $\mathbf{H}_2$) using Robieux's theorem [4]:

$$\eta = \frac{\left| \iint_S (\mathbf{E}_1 \times \mathbf{H}_2 - \mathbf{E}_2 \times \mathbf{H}_1) \cdot dS \right|^2}{4P_1P_2} \tag{8-29}$$

where P_1 and P_2 are the input powers to produce the fields and η is the efficiency. Equation (8-29) is the magnitude squared of Eq. (2-35), the reactance equation equivalence applied to Eq. (1-55) for the coupling between two antennas S_{21}. The finite size of the feed causes spillover. The extent of amplitude and phase mismatch between the two fields determines the efficiency. By illuminating the reflector with a cross-polarized wave, we compute the cross-polarization radiation level through its field match [Eq. (8-29)].

We maximize efficiency [Eq. (8-29)] by conjugate-matching the focal plane fields with the feed fields. Corrugated horns can be designed by expanding the focal plane

fields in axial hybrid modes of the horn and mode matching [22,23]. Wood [4] expands the reflector and feed fields in spherical harmonics and matches them at a boundary. Both sets of fields can be approximated very well by just a few terms, and this method can handle dual-reflector and offset reflector systems as well as axisymmetric prime focus reflectors.

We can feed the reflector with an array to match the focal plane fields [24–26]. The array samples the focal plane field and conjugate-matches it so that the powers sum in phase. The array can form multiple beams and also correct reflector aberrations [24]. By using the multiple feeds of the array, coma can be reduced for scanned beams and efficiency improved. However, quantization of the array element locations and excitations, amplitude, and phase reduces efficiency and raises the sidelobe level [27].

We apply Eq. (1-55) for the coupling between two antennas to determine the feeding coefficients of an array feed for a dish. Assume an incident field distribution on the reflector that includes the incident wave direction and the desired aperture distribution for the reflector. Using physical optics, we calculate the currents induced on the reflector surface. If the reflector has significant curvature so that the patches face each other, iterative PO can be used to account for their interaction. We calculate the fields radiated by each feed on the reflector surface and apply Eq. (1-55) to calculate coupling. This method applies the feed pattern to the calculation instead of the point matching used in a focal plane solution. Similar to scanning of an array, we use conjugative matching for the feed array elements to produce the beam desired. This method can determine array feed element amplitude and phase for any composite reflector aperture distribution that includes aperture distribution to control sidelobes or include multiple beams. The method reduces coma to the minimum possible with a given array.

Analysis finds the array distribution desired, but we do not achieve this distribution merely by designing the feed network to produce these amplitudes and phases because the feed elements have significant mutual coupling. We need to include the effect of the paraboloidal reflector when computing mutual coupling because the field radiated by one feed induces currents on the reflector that couple to other feed elements. Below we show that the effect of the reflector diminishes as the reflector diameter increases. If the mutual coupling is significant whether direct or due to the reflector, we need to apply the corrections given in Section 3-11 to adjust the feeding coefficients of the array.

8-9 FEED MISMATCH DUE TO THE REFLECTOR

The feed receives some of its transmitted power because it reflects from the parabola and returns as a mismatch at the feed terminals. We calculate the reflected field at the feed by using surface currents and the magnetic vector potential. The only significant contribution comes from areas near where the normal of the reflector points at the feed. Around every other point, the phase of the reflection varies rapidly and cancels and we need to consider only points of stationary phase. We calculate the reflection from each point of stationary phase from [2]

$$\Gamma = -j\frac{G_f(\rho_0)}{4k\rho_0}\sqrt{\frac{\rho_1\rho_2}{(\rho_1+\rho_0)(\rho_2+\rho_0)}}e^{-j2k\rho_0} \tag{8-30}$$

where Γ is the reflection coefficient, ρ_0 the distance to the stationary phase point, $G_f(\rho_0)$ the feed gain in the direction of ρ_0, and ρ_1 and ρ_2 the radiuses of curvature of the reflector at ρ_0. The vertex is the only point of stationary phase on a paraboloidal reflector: $\rho_1 = \rho_2 = -2f$ and $\rho_0 = f$. Equation (8-30) reduces to

$$\Gamma = -j\frac{G_f(0)}{2kf}e^{-j2kf} \tag{8-31}$$

Example Suppose that we have a reflector with $f/D = 0.40$. Compute reflector mismatch for a source with its 10-dB beamwidth equal to the reflector subtended angle.

Half subtended angle [Eq. (8-2)] $\psi_0 = 2\ \tan(1/1.6) = 64^\circ$. By using the feed approximation $\cos^{2N}(\theta/2)$, we have

$$N = \frac{\log 0.1}{2\log\cos(64^\circ/2)} = 6.98$$

The feed gain at the boresight is $N + 1$ [Eq. (1-20*c*)]:

$$\text{[Eq. (8-31)]} \qquad |\Gamma| = \frac{8\lambda}{4\pi f} = 1.59\frac{\lambda}{D}$$

Increasing the reflector diameter in wavelengths decreases the reaction of the reflector on the feed. For example, given a 3-m reflector at 4 GHz, we calculate reflector reflection coefficient as 0.04, or VSWR = 1.08.

We can express the reflector reflection of a paraboloidal reflector as

$$|\Gamma| = V\frac{\lambda}{D} \tag{8-32}$$

and calculate Scale 8-8 of V versus f/D for feeds with 10-dB beamwidths equal to the reflector subtended angle. Higher reflector f/D values produce larger feed reflections, since the feed gain increases faster than the reduced area of the reflector seen from the feed.

Narrowband corrections to these reflections can be designed by using a vertex plate (Silver [2]) or by designing sets of concentric ring ridges in the reflector (Wood [4]). The rings can match the feed at more than one frequency. By any of these methods, the free-space mismatch of the feed could be corrected for, but, of course, the feed itself can be mismatched to compensate for the reflector reaction.

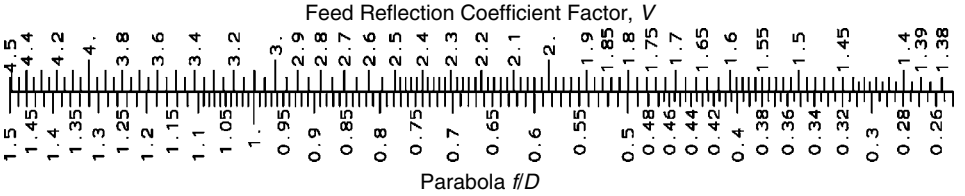

SCALE 8-8 Feed reflection scale factor V given f/D.

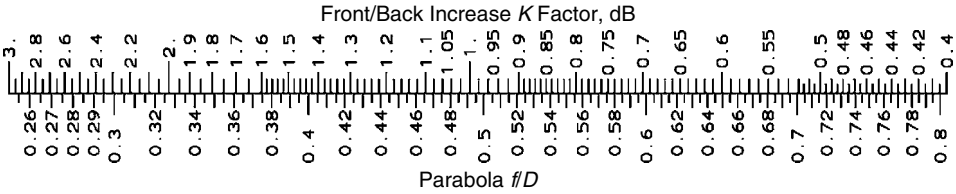

SCALE 8-9 Paraboloidal reflector front-to-back ratio increase K given f/D.

8-10 FRONT-TO-BACK RATIO

Figure 2-9 illustrates the pattern response of a paraboloidal reflector and shows that the pattern behind the reflector peaks along the axis. The diffractions from all points along the rim add in-phase along the axis and produce a pattern peak. We can reduce this rim diffraction by using a rolled, serrated, or castellated edge to reduce diffraction. An absorber-lined cylindrical shroud extending out to enclose the feed will greatly reduce back radiation, including spillover, and allows the close spacing of terrestrial microwave antennas with reduced crosstalk.

For a normal truncated circular reflector rim, the following equation estimates the front-to-back ratio given the reflector gain G, the feed taper T, and feed gain G_f [28]:

$$\text{F/B} = G + T + K - G_f \qquad \text{dB} \tag{8-33}$$

The constant K, given by Scale 8-9, is related to f/D:

$$K = 10 \log \left[1 + \frac{1}{(4f/D)^2} \right] \tag{8-34}$$

Example Estimate F/B for a reflector with $f/D = 0.34$ and 40 dB of gain.

We read the feed subtended angle from Scale 8-1 to be 143°. A 10-dB edge taper feed has a gain of about 8.1, found from Scale 1-2. Using Eq. (8-33), we estimate $\text{F/B} = 40 + 10 + 1.9 - 8.1 = 43.8$ dB.

8-11 OFFSET-FED REFLECTOR

Moving the feed out of the aperture eliminates some of the problems with axisymmetrical reflectors. Blockage losses and diffraction-caused sidelobes and cross-polarization disappear. We can increase the size of the feed structure and include more if not all of the receiver with the feed. For example, the reflector may be deployed from a satellite, with the feed mounted on the main satellite body.

Figure 8-7 shows the offset-fed reflector geometry. We form the reflector out of a piece of a larger paraboloid. Every piece of the paraboloidal reflector converts spherical waves from the focus into a plane wave moving parallel with its axis. We point the feed toward the center of the reflector to reduce the spillover, but we still locate the feed phase center at the focus of the reflector. The aperture plane projects to a circle, although the rim shape is an ellipse. ψ_0 is the angle from the axis of the parabola to